Ultrasonics 52 (2012) 996–1004

Contents lists available at SciVerse ScienceDirect

Ultrasonics

journal homepage: www.elsevier.com/locate/ultras

Eigenspace-based minimum variance beamformer combined with Wiener postfilter for medical ultrasound imaging

Xing Zeng, Cheng Chen, Yuanyuan Wang *

Department of Electronic Engineering, Fudan University, Shanghai 200433, China

ARTICLE INFO

Article history:
Received 15 May 2012
Received in revised form 31 July 2012
Accepted 31 July 2012
Available online 8 August 2012

Keywords:
Eigenspace
Wiener postfilter
Beamformer
Medical ultrasound imaging
Imaging resolution and contrast

ABSTRACT

In this paper, a new beamformer which combines the eigenspace-based minimum variance (ESBMV) beamformer with the Wiener postfilter is proposed for medical ultrasound imaging. The primary goal of this work is to further improve the medical ultrasound imaging quality on the basis of the ESBMV beamformer. In this method, we optimize the ESBMV weights with a Wiener postfilter. With the optimization of the Wiener postfilter, the output power of the new beamformer becomes closer to the actual signal power at the imaging point than the ESBMV beamformer. Different from the ordinary Wiener postfilter, the output signal and noise power needed in calculating the Wiener postfilter are estimated respectively by the orthogonal signal subspace and noise subspace constructed from the eigenstructure of the sample covariance matrix.

We demonstrate the performance of the new beamformer when resolving point scatterers and cyst phantom using both simulated data and experimental data and compare it with the delay-and-sum (DAS), the minimum variance (MV) and the ESBMV beamformer. We use the full width at half maximum (FWHM) and the peak-side-lobe level (PSL) to quantify the performance of imaging resolution and the contrast ratio (CR) to quantify the performance of imaging contrast. The FWHM of the new beamformer is only 15%, 50% and 50% of those of the DAS, MV and ESBMV beamformer, while the PSL is 127.2 dB, 115 dB and 60 dB lower. What is more, an improvement of 239.8%, 232.5% and 32.9% in CR using simulated data and an improvement of 814%, 1410.7% and 86.7% in CR using experimental data are achieved compared to the DAS, MV and ESBMV beamformer respectively. In addition, the effect of the sound speed error is investigated by artificially overestimating the speed used in calculating the propagation delay and the results show that the new beamformer provides better robustness against the sound speed errors. Therefore, the proposed beamformer offers a better performance than the DAS, MV and ESBMV beamformer, showing its potential in medical ultrasound imaging.

1. Introduction

In medical ultrasound imaging, beamforming is generally carried out by the delay-and-sum (DAS) method. Due to the predefined, fixed, and data-independent apodization weights, the beam output of the DAS beamformer has a wide mainlobe and high sidelobe levels, leading to a low resolution and weak suppression of interference.

Adaptive beamformers, which are widely used in other fields of array signal processing such as wireless communication, radar and sonar [1–5], have recently been introduced into medical ultrasound imaging to improve imaging resolution. In contrast to the predetermined, apodization weights used in the DAS beamformer, the adaptive beamformer actively updates a set of new apodization weights for each point in the image using the characteristics of the array signal. So the adaptive beamformer can bring improvement in resolution.

The most widely used method is the minimum variance (MV) beamformer originally introduced by Capon in 1969 [6]. The weights of the MV beamformer are calculated by minimizing the power of the beamformer output subject to the constraint that the beamformer must exhibit the given response in the look-direction. Several methods have been proposed in order to improve the MV beamformer during the past decades. Mann [7] introduced the Frost beamformer in 2002. Sasso and Cohen-Bacrie [8] introduced the spatial smoothing technique to decorrelate the on-axis and off-axis signals and obtained a well-conditioned covariance matrix. Diagonal loading [9] was also applied to the estimation of the covariance matrix by Synnevåg et al. to ensure its robustness. In [10], they also proposed a temporal averaged MV beamformer, wherein temporal averaging together with spatial smoothing was used to retain the speckle statistics.

* Corresponding author. Tel./fax: +86 21 65643526.
E-mail address: yywang@fudan.edu.cn (Y. Wang).

0041-624X/$ - see front matter © 2012 Elsevier B.V. All rights reserved.
http://dx.doi.org/10.1016/j.ultras.2012.07.012

The MV beamformer offers a better resolution than the DAS beamformer. However, the improvement in the contrast has not yet been satisfactory. Thus eigenspace-based techniques have been proposed. These methods utilize the fact that the covariance matrix can be divided into two orthogonal subspaces: the signal subspace and the noise subspace [11]. The signal subspace represents the information of the mainlobe signals while the noise subspace corresponds to the sidelobe signals. In the eigenspace-based minimum variance (ESBMV) beamformer proposed by Asl and Mahloojifar in [12], the weights of the beamformer are calculated by projecting the MV weights onto the constructed signal subspace. In this way, the contribution of the sidelobe signals is greatly reduced while the contribution of the interest signals remains, which leads to a significant improvement in contrast.

As the imaging resolution is determined mainly by the mainlobe width, the imaging resolution of the ESBMV beamformer is almost as same as the MV beamformer. In order to achieve a further improvement in imaging resolution while maintain the good imaging contrast of the ESBMV beamformer, we introduce the Wiener postfilter [13] into the ESBMV beamformer and propose a new beamformer in this paper. We call the new beamformer ESB-Wiener beamformer for simplicity. In the ESB-Wiener beamformer, the weights of the ESBMV beamformer are optimized with a Wiener postfilter. For any given distortionless beamformer, the Wiener postfilter is determined by minimizing the mean square error (MSE) between the output and the true signal power [14]. It will be proved in the later section that with the optimization of the Wiener postfilter, the output power of the ESB-Wiener beamformer is closer to the true signal power than the ESBMV beamformer.

The main problem in implementing the Wiener postfilter is that it needs to get accurate estimations of the expected signal power and the output noise power to calculate the Wiener postfilter. However, this information is generally not available. In [14], the expected signal power and the output noise power are estimated by the magnitude-squared MV output and the mean squared error between the MV output and sensor signals. This way of estimating the signal power and the output noise power is usually not accurate enough. In our proposed ESB-Wiener beamformer, they are estimated respectively using the signal covariance matrix and noise covariance matrix constructed by the signal subspace and noise subspace, which provides much more accurate estimations than the method used in [14].

It can be seen from the later results using both simulated data and experimental data that the ESB-Wiener beamformer achieves better imaging resolution and contrast compared to the DAS, MV and ESBMV beamformer. What is more, it provides better robustness against the sound speed errors due to medium inhomogeneities.

The outline of this manuscript is as follows. The background is presented in Section 2, including the signal sensor model, the MV beamformer and the Wiener postfilter. The method of the proposed beamformer is introduced in Section 3. The implementation of the new beamformer is summarized in Section 4. The results of the different beamformers applied to simulated data and experimental data are shown in Section 5. Finally, discussion about the new beamformer and conclusion are given in Section 6.

2. Background

2.1. Minimum variance beamformer

We assume a linear array of M elements and the signal received at time instant k is given by:

$$\mathbf{x}(k) = s(k)\mathbf{a} + p(k), \tag{1}$$

where $s(k)$, $\mathbf{p}(k)$ indicate the desired signal and the sum of interference and noise and $\mathbf{a}$ is the steering vector corresponding to the desired signal. For broadband signals, the time-delays cannot be expressed as complex exponentials, so we first apply appropriate delays on each sensor to focus in the direction of the transmitted beam. In this way, the steering vector in (1) simply becomes $\mathbf{a} = [1, 1, \cdots, 1]^T$. As in [14], we assume a model in which $s(k)$ is uncorrelated with $\mathbf{p}(k)$. The weights of MV beamformer are determined by minimizing the variance of the beamformer output under the constraint that the signal reflecting from the direction of interest is passed without distortion, that is

$$\mathbf{w}_{\mathrm{MV}} = \arg\min_{\mathbf{w}} \mathbf{w}^H\mathbf{R}\mathbf{w} \qquad \text{subject to} \quad \mathbf{w}^H\mathbf{a} = 1. \tag{2}$$

The solution to (2) is given by

$$\mathbf{w}_{\mathrm{MV}} = \frac{\mathbf{R}^{-1}\mathbf{a}}{\mathbf{a}^H\mathbf{R}^{-1}\mathbf{a}}. \tag{3}$$

The covariance matrix is unknown and usually placed by the sample covariance matrix:

$$\mathbf{R} = \mathbf{x}^d\mathbf{x}^{dH}, \tag{4}$$

where $\mathbf{x}^d = [x_1^d(k), x_2^d(k), \cdots, x_M^d(k)]^T$ denotes the delayed sensor signals. If we directly use (4) to compute the covariance matrix, it is easy to get an ill-conditioned matrix not suitable for the inversion required in (3). So we divide the array into overlapping subarrays which are averaged to obtain the covariance matrix estimation, which is so-called spatial smoothing [8]. Then the covariance matrix is estimated as:

$$\mathbf{R} = \frac{1}{P}\sum_{p=1}^{P}\mathbf{x}_p^d\mathbf{x}_p^{dH}, \tag{5}$$

where $P = M - L + 1$ is the number of overlapping subarrays, L is the subarray length and $\mathbf{x}_p^d = [x_p^d(k), x_{p+1}^d(k), \cdots, x_{p+L-1}^d(k)]^T$ denotes the signal vector of the dth subarray.

Commonly, a large number of samples are required to obtain a stable covariance matrix. A common way to increase robustness of the covariance matrix using only a few temporal samples is to add a constant, ε, into the diagonal of the covariance matrix, replacing $\mathbf{R}$ with $\mathbf{R} + \varepsilon\mathbf{I}$ ($\mathbf{I}$ represents the unit matrix). This method is called the diagonal loading (DL) technique. The loading factor ε is usually set to be δ times the power in the received signals [9,15]:

$$\varepsilon = \delta \cdot \mathrm{trace}\{\mathbf{R}\}. \tag{6}$$

After the estimation of the covariance matrix, the $L \times 1$ MV weights are got by expression (3). Then, the final output of the MV beamformer is given by:

$$y(k) = \frac{1}{M-L+1}\sum_{p=1}^{M-L+1}\mathbf{w}^H(k)\mathbf{x}_p^d(k). \tag{7}$$

2.2. Wiener postfilter

For any given distortionless beamformer satisfying $\mathbf{w}^H\mathbf{a} = 1$, the Wiener postfilter is determined by minimizing the mean square error between the beamformer output and the expected signal, which can be expressed as:

$$H_{\mathrm{Wiener}} = \arg\min_{\mathbf{w}} E\{|s - H\mathbf{w}^H\mathbf{x}|^2\}. \tag{8}$$

The solution to (5) is:

$$H_{\mathrm{Wiener}} = \frac{|s|^2}{\mathbf{w}^H\mathbf{R}\mathbf{w}} = \frac{|s|^2}{|s|^2 + \mathbf{w}^H\mathbf{R}_p\mathbf{w}}. \tag{9}$$

It is clear that estimations of the signal power $|s|^2$ and output noise power $\mathbf{w}^H\mathbf{R}_p\mathbf{w}$ are needed. In [14], the signal power is estimated as:

$$|s|^2 = |y(k)|^2, \tag{10}$$

where $y(k)$ is the output of the beamformer, it can be any distortionless beamformer like DAS or MV beamformer. And the output noise power is estimated as:

$$E\{|\mathbf{w}^H p|^2\} = \mathbf{w}^H\mathbf{R}_p\mathbf{w}, \tag{11}$$

where the noise covariance matrix $\mathbf{R}_p$ is calculated by:

$$\mathbf{R}_p = \frac{1}{M}\sum_{m=1}^{M}\left(x_m^d(k) - y(k)\right)^2 * \mathbf{I}. \tag{12}$$

3. Method

In the ESB-Wiener beamformer, the covariance matrix $\mathbf{R}$ is firstly eigen decomposed to a signal subspace and a noise subspace, that is:

$$\mathbf{R} = \mathbf{U}\Lambda\mathbf{U}^H = \mathbf{U}_s\Lambda_s\mathbf{U}_s^H + \mathbf{U}_p\Lambda_p\mathbf{U}_p^H = \mathbf{R}_s + \mathbf{R}_p, \tag{13}$$

where $\Lambda = \mathrm{diag}[\lambda_1, \lambda_2, \cdots, \lambda_L]$, in which $\lambda_1 \geqslant \lambda_2 \geqslant \cdots \geqslant \lambda_L$ are the eigenvalues in descending order, and $\mathbf{U} = [\mathbf{v}_1, \mathbf{v}_2, \cdots, \mathbf{v}_L]$ is constructed by the orthonormal eigenvector $\mathbf{v}_i$ ($i = 1, 2, \ldots, L$) corresponding to λ_i. Similarly, $\mathbf{U}_s = [\mathbf{v}_1, \mathbf{v}_2, \cdots, \mathbf{v}_{N\_sig}]$ and $\mathbf{U}_p = [\mathbf{v}_{N\_sig+1}, \mathbf{v}_{N\_sig+2}, \cdots, \mathbf{v}_L]$ are the signal subspace related to the largest *N_sig* eigenvalues and the noise subspace related to the remaining smaller eigenvalues.

The number of the eigenvectors used to construct the signal subspace varies at each focal point and depends on the relative energy of the mainlobe signals and sidelobe signals. A simple way to construct the signal subspace is to choose those eigenvectors whose related eigenvalues are larger than α times the largest eigenvalue or β times the smallest eigenvalue. In practice, α is always chosen from 0.1 to 0.5 while β is always chosen from 10 to 50.

Secondly, we get the ESBMV weights by projecting the MV weights onto the signal subspace [12]:

$$\mathbf{w}_{\mathrm{ESBMV}} = \mathbf{U}_s\mathbf{U}_s^H\mathbf{w}_{\mathrm{MV}}. \tag{14}$$

Then, the output power of the ESBMV beamformer becomes:

$$\begin{aligned}|y_{\mathrm{ESBMV}}|^2 &= (\mathbf{x}^{dH}\mathbf{w}_{\mathrm{ESBMV}})^H\mathbf{x}^{dH}\mathbf{w}_{\mathrm{ESBMV}} = \mathbf{w}_{\mathrm{ESBMV}}^H\mathbf{x}^d\mathbf{x}^{dH}\mathbf{w}_{\mathrm{ESBMV}}\\ &= \mathbf{w}_{\mathrm{ESBMV}}^H\mathbf{R}\mathbf{w}_{\mathrm{ESBMV}}\\ &= \mathbf{w}_{\mathrm{MV}}^H\mathbf{U}_s\mathbf{U}_s^H(\mathbf{U}_s\Lambda_s^{-1}\mathbf{U}_s^H + \mathbf{U}_p\Lambda_p^{-1}\mathbf{U}_p^H)\mathbf{U}_s\mathbf{U}_s^H\mathbf{w}_{\mathrm{MV}}\\ &= |s|^2 + \mathbf{w}_{\mathrm{MV}}^H\mathbf{U}_s\mathbf{U}_s^H\mathbf{U}_p\Lambda_p^{-1}\mathbf{U}_p^H\mathbf{U}_s\mathbf{U}_s^H\mathbf{w}_{\mathrm{MV}}\end{aligned} \tag{15}$$

The second term of (15) indicates the noise output power. Ideally, the signal subspace $\mathbf{U}_s$ is orthogonal to the noise subspace $\mathbf{U}_p$, so the noise output power will be completely suppressed. However, since a correct estimation of the signal subspace is not easily obtained, in practice the output power of the ESBMV beamformer becomes:

$$|y_{\mathrm{ESBMV}}|^2 = |s|^2 + \mathbf{w}_{\mathrm{ESBMV}}^H\mathbf{R}_p\mathbf{w}_{\mathrm{ESBMV}}. \tag{16}$$

Thirdly, the ESBMV weights are optimized with a Wiener postfilter, that is:

$$\mathbf{w}_{\mathrm{ESB-Wiener}} = \frac{|s|^2}{|s|^2 + \mathbf{w}_{\mathrm{ESBMV}}^H\mathbf{R}_p\mathbf{w}_{\mathrm{ESBMV}}} \cdot \mathbf{w}_{\mathrm{ESBMV}}. \tag{17}$$

In this way, the output power of the beamformer is:

$$\begin{aligned}|y_{\mathrm{ESB-Wiener}}|^2 &= \mathbf{w}_{\mathrm{ESB-Wiener}}^H\mathbf{R}\mathbf{w}_{\mathrm{ESB-Wiener}}\\ &= \left(\frac{|s|^2}{|s|^2 + \mathbf{w}_{\mathrm{ESBMV}}^H\mathbf{R}_p\mathbf{w}_{\mathrm{ESBMV}}}\right)^2 \mathbf{w}_{\mathrm{ESBMV}}^H\mathbf{R}\mathbf{w}_{\mathrm{ESBMV}}\\ &= \left(\frac{|s|^2}{|s|^2 + \mathbf{w}_{\mathrm{ESBMV}}^H\mathbf{R}_p\mathbf{w}_{\mathrm{ESBMV}}}\right)^2 \left(|s|^2 + \mathbf{w}_{\mathrm{ESBMV}}^H\mathbf{R}_p\mathbf{w}_{\mathrm{ESBMV}}\right)\\ &= \frac{|s|^4}{|s|^2 + \mathbf{w}_{\mathrm{ESBMV}}^H\mathbf{R}_p\mathbf{w}_{\mathrm{ESBMV}}}\\ &= |s|^2 - \frac{\mathbf{w}_{\mathrm{ESBMV}}^H\mathbf{R}_p\mathbf{w}_{\mathrm{ESBMV}}}{1 + \frac{\mathbf{w}_{\mathrm{ESBMV}}^H\mathbf{R}_p\mathbf{w}_{\mathrm{ESBMV}}}{|s|^2}}.\end{aligned} \tag{18}$$

The performance of the ESBMV beamformer is determined by the accuracy of the estimation of the signal subspace. If the estimation is incorrect, it will lead to a relative large output noise power $\mathbf{w}_{\mathrm{ESBMV}}^H\mathbf{R}_p\mathbf{w}_{\mathrm{ESBMV}}$.

The effects of the Wiener postfilter can be explained as follows.

If the signal power is much larger than the output noise power, the ratio of the output noise power and the signal power $\mathbf{w}_{\mathrm{ESBMV}}^H\mathbf{R}_p\mathbf{w}_{\mathrm{ESBMV}}/|s|^2$ is very small and can be treated as 0. So both the ESBMV output power $|s|^2 + \mathbf{w}_{\mathrm{ESBMV}}^H\mathbf{R}_p\mathbf{w}_{\mathrm{ESBMV}}$ and the ESB-Wiener output power are very close to the true signal power $|s|^2$.

If the output noise power is much larger than the signal power, the ratio of the output noise power and the signal power $\mathbf{w}_{\mathrm{ESBMV}}^H\mathbf{R}_p\mathbf{w}_{\mathrm{ESBMV}}/|s|^2$ becomes quite large. With a denominator much larger than 1, the second term of the expression (18) will be greatly reduced. This means the output power of the ESB-Wiener beamformer is closer to the real signal power $|s|^2$ than the ESBMV output power $|s|^2 + \mathbf{w}_{\mathrm{ESBMV}}^H\mathbf{R}_p\mathbf{w}_{\mathrm{ESBMV}}$.

It will be shown in Section 5 that the ESB-Wiener beamformer has lower sidelobes and a narrower mainlobe than the ESBMV beamformer.

4. Implementation of the algorithm

In summary, for each point in the imaging region, the algorithm can be implemented by going through the following procedure.

(1) Calculate the delay time for each channel of the array according to the transmitting delay and apply it to the received signals.
(2) Divide the array into P subarrays with a length of L and use formula (5) and (6) to construct the sample covariance matrix $\mathbf{R}$.
(3) Eigen decompose the covariance matrix $\mathbf{R}$ into a signal subspace and a noise subspace as shown in formula (13).
(4) Get the ESBMV weights by projecting the MV weights onto the signal subspace using formula (14).
(5) Use the signal subspace and the noise subspace got by procedure (3) and the ESBMV weights got by procedure (4) to estimate the signal power and output noise power in the Wiener postfilter.
(6) Optimize the ESBMV weights with the Wiener postfilter to get the ESB-Wiener weights using formula (17).
(7) Get the output of the beamformer using formula (7), but the weights are not the MV weights but the ESB-Wiener weights got by procedure (6).

For each imaging point, we repeat the above steps and get a matrix of beamformed output. At last, a final imaging result is shown by using the matrix with different dynamics.

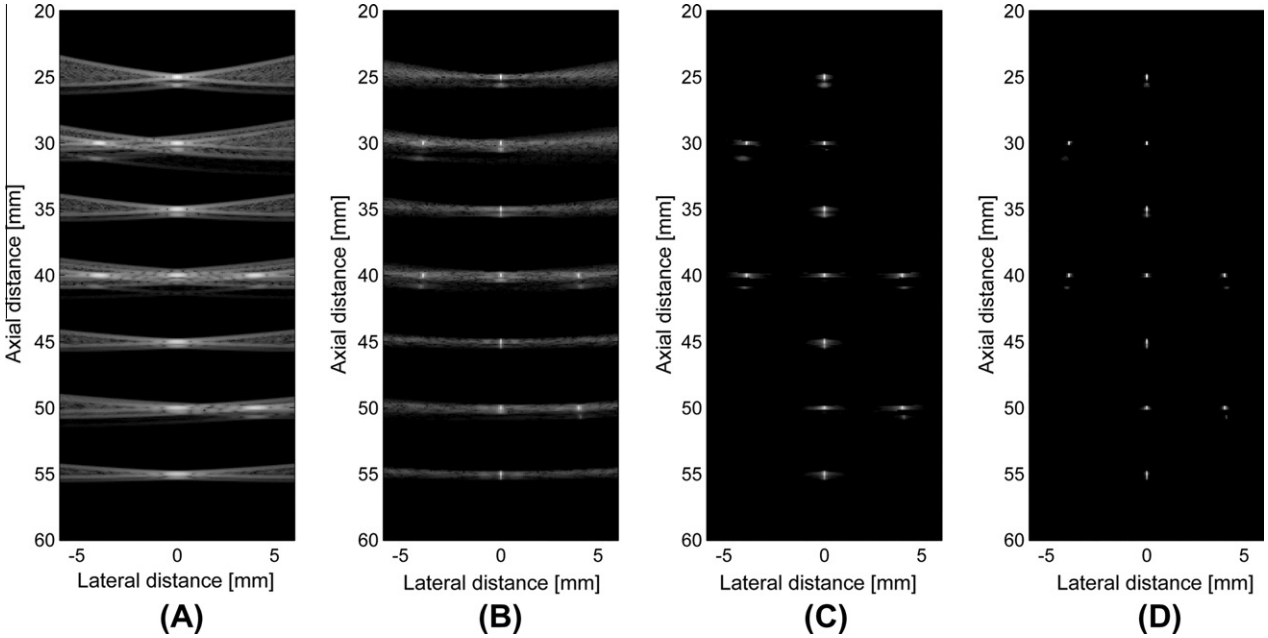

Fig. 1. Beamformed responses of 11 point targets using an 128-elements, 7-MHz linear array. (A) DAS, (B) MV, (C) ESBMV, and (D) ESB-Wiener. All images are shown with a dynamic range of 70 dB.

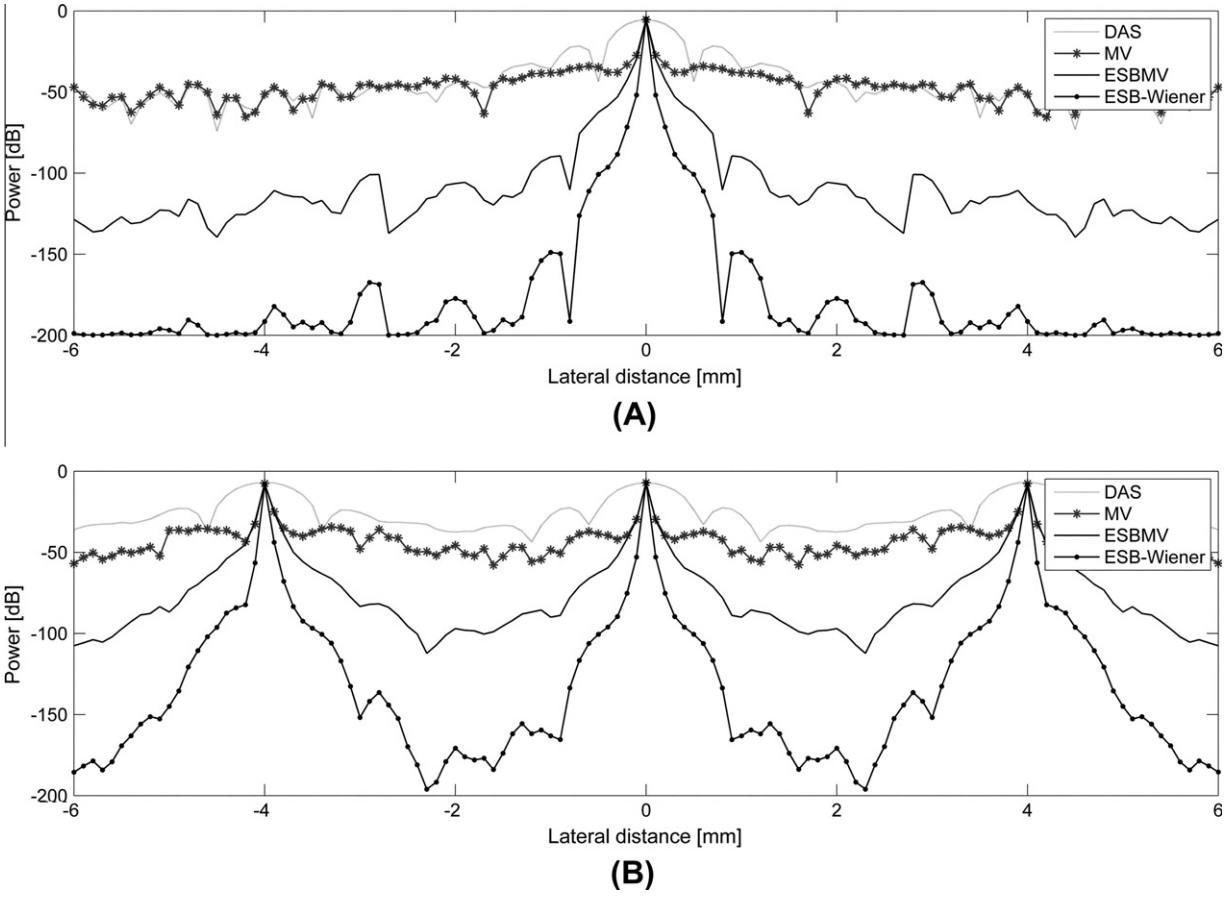

Fig. 2. Lateral variation at depths $z = 25$ mm (A), and 40 mm (B) of the beamformed responses.

5. Simulation and experimental results

In this section, we demonstrated the performance of the ESB-Wiener beamformer when resolving point targets for simulated and experimental data and compared it to those of the DAS, MV and ESBMV beamformer for different parameters. We also compared the performance of all beamformers when resolving cysts in speckle. All simulated data are acquired with the ultrasound

Table 1
Full width at half maximum (FWHM[a]) and peak-side-lobe (PSL[b]) for the beamformed responses at $z = 25$ mm.

Beamformer	FWHM (mm)	PSL (dB)
DAS	0.20	−21.67
MV	0.06	−34.07
ESBMV	0.06	−89.35
ESB-Wiener	0.03	−148.9

[a] FWHM means the full width at half maximum.
[b] PSL means the peak value of the first sidelobe.

simulation phantom Field II [16] and all experimental data are from Medical Engineering Program of Electrical and Electronic Engineering Department of University of Hongkong. In order to short down the emission time, we chose the plane-wave emission [17] rather than the widely used synthetic aperture emission [18].

In the simulation cases, a 7-MHz, 128-element linear array transducer with $\lambda/2$-spacing was used and the sampling rate was 100 MHz. In the practical cases, a 5-MHz, 128-element linear array transducer with an element pitch of 0.308 mm was used and the sampling rate was 40 MHz. The fractional bandwith of the transducer was 60% and the excitation pulse was a two-cycle sinusoid at the central frequency. A subarray size of $L = 48$ was used and the loading factor ε was set to be 0.1 times the power in the received signals. In the simulation cases, a zero-mean, Gaussian distributed noise with a SNR of 60 dB was added to each of the sensor signals before beamforming.

We simulated 11 point scatterers at seven different depths to compare the beamformers in terms of the resolution and sidelobe level. The contrast performance was evaluated by resolving an anechoic cyst in a speckle pattern. Furthermore, we presented the point target and cyst imaging results of different beamformers using the experimental ultrasound data. At last, the robustness of all beamformers was investigated by artificially introducing sound speed errors during beamforming.

5.1. Simulated data: point targets

The beamformed responses of 11 point targets located at depths from 20 to 60 mm are shown in Fig. 1, with a dynamic range of 70 dB. It can be seen that the DAS beamformer has a wide mainlobe and high sidelobes. The MV beamformer provides a narrower mainlobe than the DAS beamformer. The ESBMV beamformer lowers down sidelobes but the mainlobe is still as wide as the MV beamformer. It is clear from Fig. 1D that the ESB-Wiener beamformer has both a narrow mainlobe and low sidelobes.

The lateral variation of the beamformed responses are shown in Fig. 2A and B at the depths $z = \{25, 40\}$ mm. At the depth $z = 25$ mm, the mainlobe width of the ESB-Wiener beamformer is less than half of that of the ESBMV beamformer. Moreover, the ESB-Wiener beamfomer suppresses the sidelobes by more than 100 dB compared to the ESBMV beamformer.

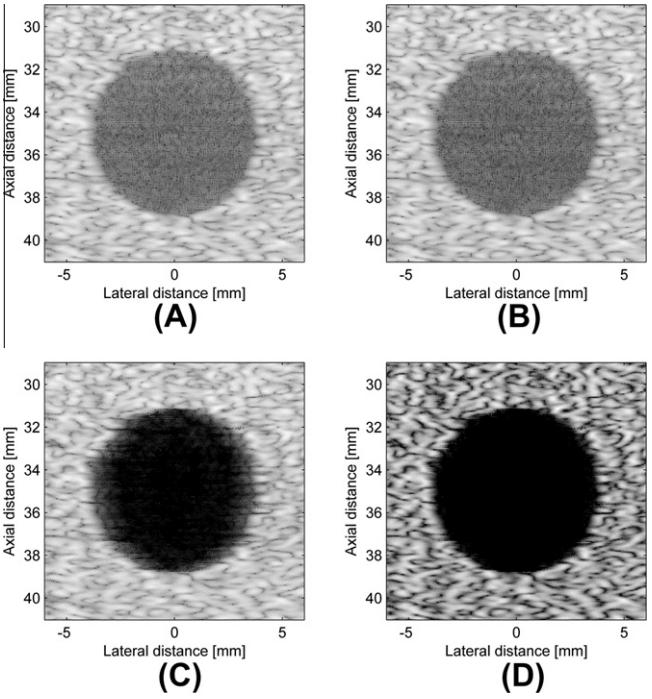

Fig. 4. Beamformed responses of cyst using an 128-elements, 7-MHz linear array. (A) DAS, (B) MV, (C) ESBMV, and (D) ESB-Wiener. All images are shown with a dynamic range of 80 dB.

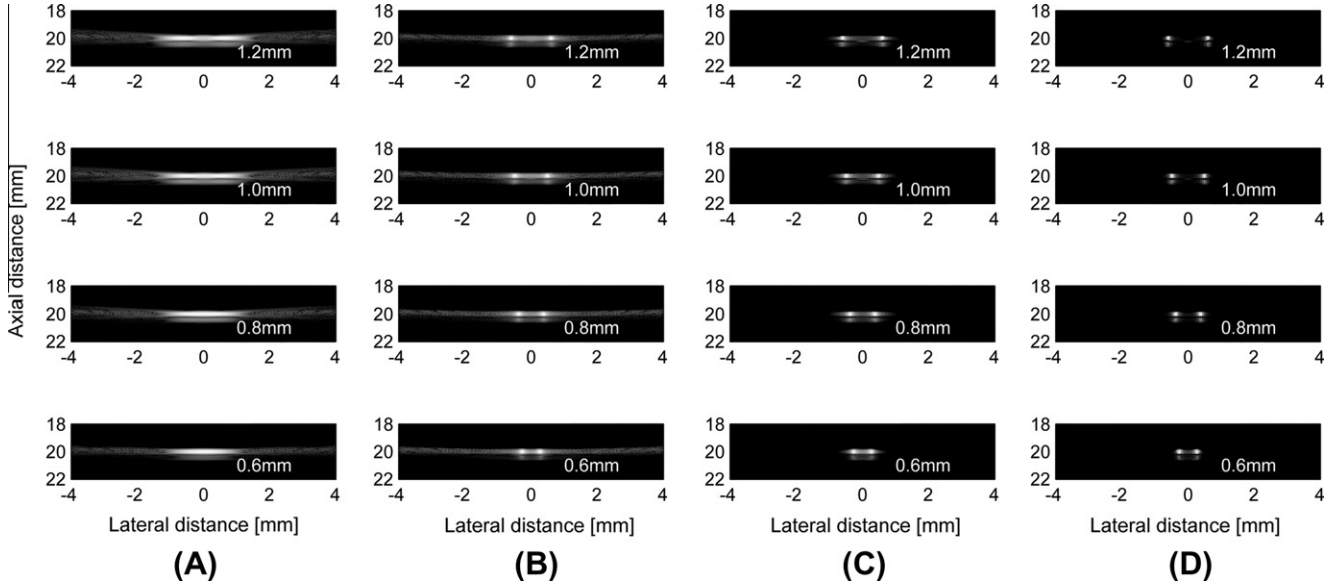

Fig. 3. Beamformed responses of two near point scatterers at different distances. (A) DAS, (B) MV, (C) ESBMV, and (D) ESB-Wiener. The distance is indicated on the lower right of each image. All images are shown with a dynamic range of 70 dB.

Table 2
Contrast ratio of the simulated cyst for different beamformers.

Beamformer	Mean intensity outside the cyst (dB)	Mean intensity inside the cyst (dB)	CR[a] (dB)
DAS	−12.12	−26.64	14.52
MV	−12.33	−27.17	14.84
ESBMV	−13.26	−50.38	37.12
ESB-Wiener	−22.64	−71.99	49.35

[a] CR = Mean intensity outside the cyst − Mean intensity inside the cyst.

The resolution improvements were quantified using the full width at half maximum (FWHM) and peak-side-lobe (PSL), which is defined as the peak value of the first sidelobe. These quantitative measures are calculated at the depth of 25 mm and are given in Table 1.

It can be seen that the FWHM of the ESB-Wiener beamformer is only 15%, 50% and 50% of that of the DAS, MV and ESBMV beamformer, while the PSL is 127.2 dB, 115 dB and 60 dB lower than the DAS, MV and ESBMV beamformer.

We also investigated the ability of the new beamformer to separate two single scatterers and the simulation results are given in Fig. 3 with comparison to other beamformers.

We can see from Fig. 3 that the DAS, MV and ESBMV beamformer fail to separate the two point scatterers at a distance of 1.2 mm. However the ESB-Wiener beamformer succeeds to separate the two points even at a distance of 0.6 mm. All the simulation results above indicate that the proposed beamformer provides a higher imaging resolution than the DAS, MV and ESBMV beamformer.

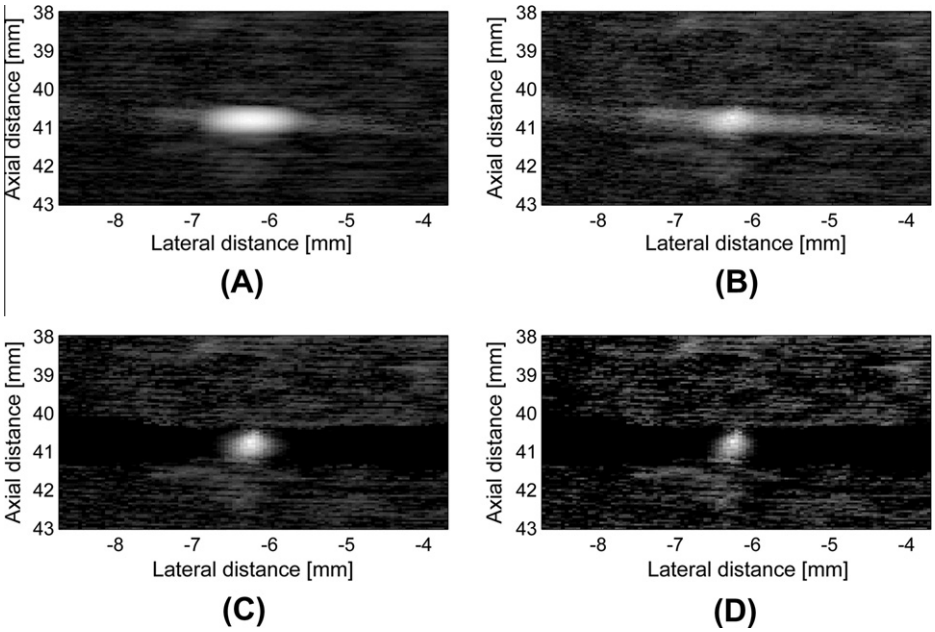

Fig. 5. Beamformed responses of a real point targets using an 128-elements, 7-MHz linear array. (A) DAS, (B) MV, (C) ESBMV, and (D) ESB-Wiener. All images are shown with a dynamic range of 40 dB.

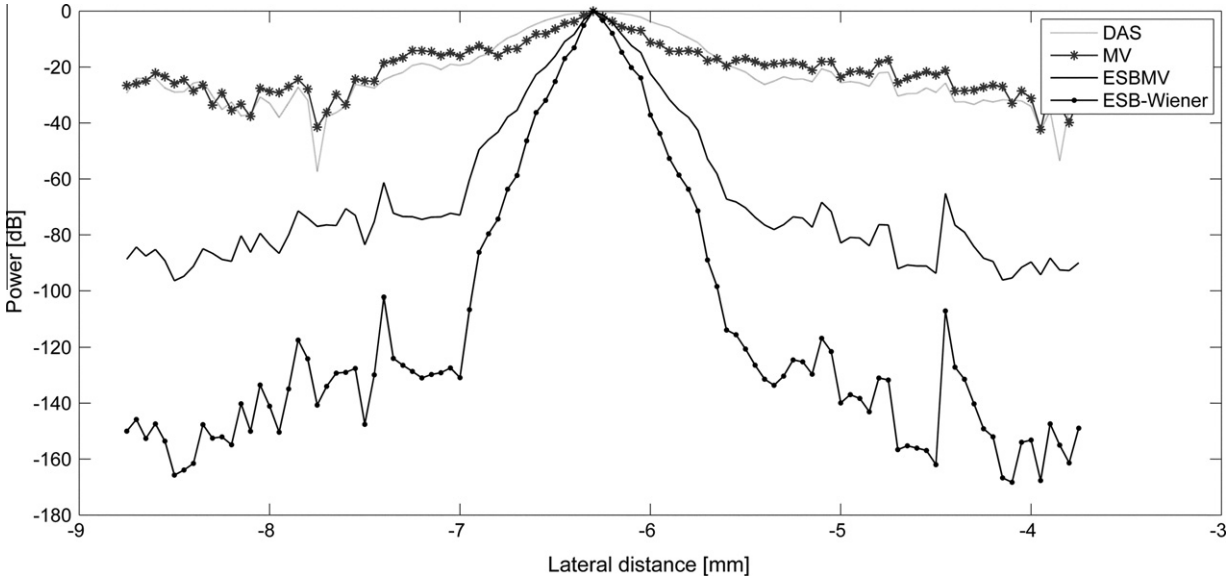

Fig. 6. Lateral variation at depths $z = 40.75$ mm of the beamformed responses in Fig. 5.

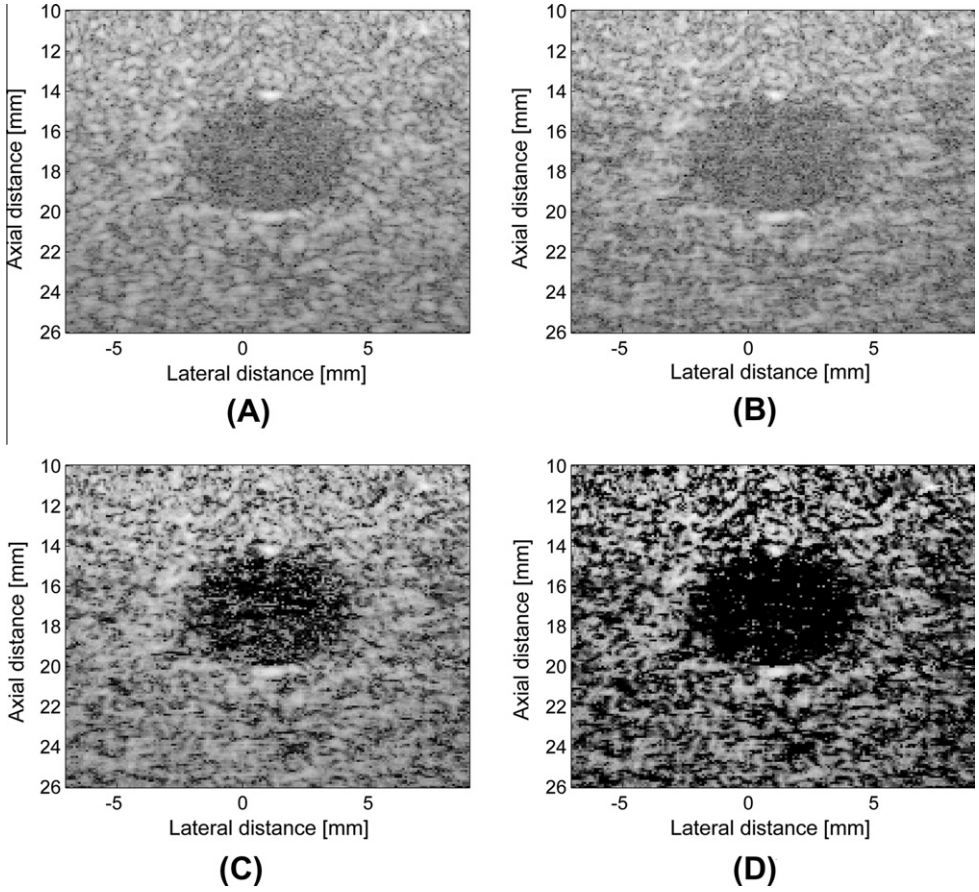

Fig. 7. Beamformed responses of a real cyst using an 128-elements, 7-MHz linear array. (A) DAS, (B) MV, (C) ESBMV, and (D) ESB-Wiener. All images are shown with a dynamic range of 80 dB.

5.2. Simulated data: cyst phantom

In this section, a circular cyst in a speckle pattern was simulated. The cyst had a radius of 4 mm and centers at $(x, y, z) = (0, 0, 35)$ mm. The speckle pattern was simulated with 10 randomly placed scatterers within a resolution cell of λ^3, where λ was the central wavelength, to ensure fully developed speckle [19]. The scattering amplitudes were Gaussian distributed.

The beamformed responses of the cyst phantom are shown in Fig. 4, with a dynamic range of 80 dB. We can see that both the DAS and MV beamformer have a poor contrast due to the high sidelobe level, the ESBMV beamformer can provide a better contrast than the MV and DAS beamformer, but the edge of the cyst is still hard to distinguish. The ESB-Wiener beamformer have a much higher contrast and clearer edge.

We used the contrast ratio (CR) [13] to quantify the contrast performance. The CR is defined as the ratio of the mean level outside the cyst region to the mean level inside. The results are shown in Table 2. The ESB-Wiener beamformer achieves an improvement of 239.8%, 232.5% and 32.9% in CR compared to the DAS, MV and ESBMV beamformers respectively.

5.3. Experimental data: point target

An image of a point target with a radius of 0.1 mm located at depths $z = 40.75$ mm is shown in Fig. 5 to show the performance of the proposed beamformer in dealing with experimental data acquired with ultrasonic probe. Because of the high noise in the background, the image is shown with a dynamic range of only 40 dB.

It is clear from Fig. 5 that the ESB-Wiener demonstrates a better resolution compared with ESBMV, MV and DAS beamformer. The radius of the target is closest to 0.1 mm in Fig. 5D, which is the imaging result of the ESB-Wiener beamformer.

The lateral variation of the beamformed responses is shown in Fig. 6 at the depths $z = 40.75$ mm. The mainlobe width of the ESB-Wiener beamformer is narrower than that of the ESBMV beamformer and closest to the original shape of the point.

Since the point target in this simulation is not an ideal point, we did not calculate the FWHM and the PSL of the beamformers.

5.4. Experimental data: cyst phantom

An image of a cyst centers at $(x, y, z) = (1.1, 0, 17.5)$ mm is shown in Fig. 7. The image is shown with a dynamic range of 80 dB. It is clear that the ESB-Wiener beamformer offers the best contrast among all the beamformers. The cyst is quite hard to distinguish in the images beamformed by the DAS and MV beamformer. The ESBMV beamformer offers a better contrast than the former two, but the sharp of cyst is still hard to judge. The edge

Table 3
Contrast ratio of the experimental cyst for different beamformers.

Beamformer	Mean intensity outside the cyst (dB)	Mean intensity inside the cyst (dB)	CR[a] (dB)
DAS	−20.05	−22.05	2.00
MV	−20.67	−21.88	1.21
ESBMV	−24.00	−33.79	9.79
ESB-Wiener	−35.56	−53.84	18.28

[a] CR = Mean intensity outside the cyst – Mean intensity inside the cyst.

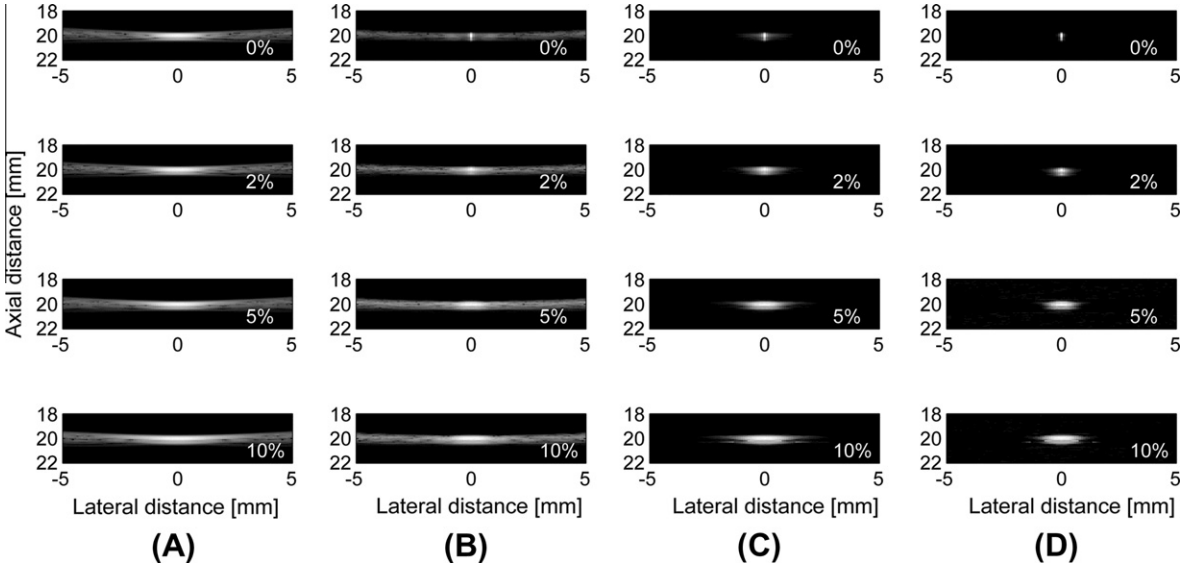

Fig. 8. Point spread functions (PSF) for the (A) DAS, (B) MV, (C) ESBMV, and (D) ESB-Wiener beamformer subjected to errors in the sound estimate. The percentage error is indicated on the lower right of each image. All images are shown with a dynamic range of 70 dB.

of cyst in Fig. 7D is much easier to distinguish than other beamformers.

We used the contrast ratio to quantify the contrast performance. The results are shown in Table 3. The CR of both the DAS and the MV beamformer are quite low. The CR of the ESBMV beamformer is a little higher. The ESB-Wiener beamformer achieves an improvement of 814%, 1410.7% and 86.7% in CR compared to the DAS, MV and ESBMV beamformers respectively.

5.5. Effects of sound speed errors

Adaptive beamformers are usually sensitive to steering vector errors [20,21]. Errors in the steering vector are common in medical ultrasound imaging, because of the inhomogeneity of tissues [22]. In this section, the effect of steering vector errors was investigated. The sound speed was assumed to be over-estimated by 0%, 2%, 5% and 10%, respectively. The point spread functions (PSFs) are shown in Fig. 8. It can be seen that both the mainlobe width and the sidelobe level degrade as the sound speed error increases, but the proposed beamformer still shows the best performance, indicating a higher robustness against the steering vector errors.

6. Discussions and conclusion

We have successfully applied the ESB-Wiener beamformer to medical ultrasound imaging and shown the great improvement in imaging resolution, contrast and robustness compared to the DAS, MV and ESBMV beamformer. The proposed method has been demonstrated on simulated radio frequency (RF) data and experimental data acquired with the actual ultrasound probe, showing its potential in medical ultrasound imaging.

It can be seen from expression (18) that although the ESB-Wiener output power is closer to the true signal power, it is smaller than the true signal power. This will somehow influence the imaging contrast, especially at the place where the signal energy is close to the noise energy. This explains why the mean intensity outside the cyst of the ESB-Wiener beamformer is lower than the ESBMV beamformer.

Acknowledgements

This work is supported by the Natural Science Foundation of China (No. 10974035) and Specialized Research Fund for the Doctoral Program of Higher Education of China (No. 20110071110017).

We appreciate Professor Alfred C.H. Yu at Medical Engineering Program of Electrical and Electronic Engineering Department of University of Hongkong for providing the experimental data of the point target and cyst used in the simulations.

References

[1] J.H. Lee, K.P. Cheng, C.C. Wang, Robust adaptive array beamforming under steering angle mismatch, Signal Processing 86 (2006) 296–309.
[2] A.D. George, J. Markwell, R. Fogarty, Real-time sonar beamforming on high-performance distributed computers, Parallel Computing 26 (2000) 1231–1252.
[3] S. Fischer, K.U. Simmer, Beamforming microphone arrays for speech acquisition in noisy environments, Speech Communication 20 (1996) 215–227.
[4] S. Chen, L. Hanzo, N.N. Ahmad, A. Wolfgang, Adaptive minimum bit error rate beamforming assisted receiver for QPSK wireless communication, Digital Signal Processing 15 (2005) 545–567.
[5] C. Xiang, D.Z. Feng, H. Lv, J. He, Y. Cao, Robust adaptive beamforming for MIMO radar, Signal Processing 90 (2010) 3185–3196.
[6] J. Capon, High-resolution frequency-wave number spectrum analysis, in: Proceedings of the IEEE, vol. 57, 1969, pp. 1408–1418.
[7] J.A. Mann, W.F. Walker, A constrained adaptive beamformer for medical ultrasound: Initial results, in: Proceedings of the 2002 International IEEE Ultrasonics Symposium, vol. 2, 2002, pp. 1807–1810.
[8] M. Sasso, C. Cohen-Bacrie, Medical ultrasound imaging using the fully adaptive beamformer, in: 2005 IEEE International Conference on Acoustics, Speech, and Signal Processing, vol. 2, 2005, pp. 489–492.
[9] J.-F. Synnevåg, A. Austeng, S. Holm, Adaptive beamforming applied to medical ultrasound imaging, IEEE Transaction on Ultrasonics, Ferroelectrics, and Frequency Control 54 (2007) 1603–1613.
[10] J.-F. Synnevåg, C.I.C. Nilsen, S. Holm, Speckle statistics in adaptive beamforming, in: Proceedings of the 2007 International IEEE Ultrasonics Symposium, 2007, pp. 1545–1548.
[11] J.-L. Yu, C.-C. Yeh, Generalized eigenspace-based beamformers, IEEE Transaction on Signal Processing 43 (1995) 2453–2461.
[12] B.M. Asl, A. Mahloojifar, Eigenspace-based minimum variance beamforming applied to medical ultrasound imaging, IEEE Transaction on Ultrasonics, Ferroelectrics, and Frequency Control 57 (2010) 2381–2390.
[13] R. Zelinski, A microphone array with adaptive post-filtering for noise reduction in reverberant rooms, in: 1988 International Conference on Acoustics, Speech, and Signal Processing, 1988, pp. 2578–2581.
[14] C.-I.C. Nilsen, S. Holm, Wiener beamforming and the coherence factor in ultrasound imaging, IEEE Transaction on Ultrasonics, Ferroelectrics, and Frequency Control 57 (2010) 1329–1346.
[15] A. Ozbek, Adaptive seismic noise and interference attenuation method, US Patent 6446008 B1, 2002.

[16] J. A. Jensen, Field: A program for simulating ultrasound systems, in: 10th Nordic-Baltic Conference on Biomedical Imaging, vol. 4, No. sup. 1, part 1, 1996, pp. 351–353.
[17] I.K. Holfort, F. Gran, J.A. Jensen, Plane wave medical ultrasound imaging using adaptive beamforming, in: 5th IEEE Sensor Array and Multichannel Signal Processing, 2008, pp. 288–292.
[18] J.A. Jensen, S.I. Nikolov, K.L. Gammelmark, M.H. Pedersen, Synthetic aperture ultrasound imaging, Ultrasonics 44 (2006) e5–e15.
[19] M. ODonnell, S.W. Flax, Phase-aberration correction using signals from point reflectors and diffuse scatterers: measurements, IEEE Transaction on Ultrasonics, Ferroelectrics, and Frequency Control 35 (1988) 768–774.
[20] C. Yoon, Y. Lee, J.H. Chang, T. Song, Y. Yoo, In vitro estimation of mean sound speed based on minimum average phase variance in medical ultrasound imaging, Ultrasonics 51 (2011) 795–802.
[21] D. Napolitano, C.-H. Chou, G. McLaughlin, T.-L. Ji, L. Mo, D. DeBusschere, R. Steins, Sound speed correction in ultrasound imaging, Ultrasonics 44 (2006) e43–e46.
[22] S.A. Goss, R.L. Johnston, F. Dunn, Comprehensive compilation of empirical ultrasonic properties of mammalian tissues, The Journal of the Acoustical Society of America 64 (1978) 423–457.